

<https://doi.org/10.1007/s10483-022-2912-6>

## A novel physics-informed framework for reconstruction of structural defects\*

Qi LI<sup>1</sup>, Fushun LIU<sup>2</sup>, Bin WANG<sup>1</sup>, D. Z. LIU<sup>3,†</sup>, Zhenghua QIAN<sup>1,†</sup>

1. State Key Laboratory of Mechanics and Control of Mechanical Structures, College of Aerospace Engineering, Nanjing University of Aeronautics and Astronautics, Nanjing 210016, China;
2. College of Engineering, Ocean University of China, Qingdao 266100, Shandong Province, China;
3. School of Engineering, University of East Anglia, Norwich NR4 7TJ, U.K.

(Received Mar. 31, 2022 / Revised Aug. 8, 2022)

**Abstract** The ultrasonic guided wave technology plays a significant role in the field of non-destructive testing as it employs acoustic waves with the advantages of high propagation efficiency and low energy consumption during the inspect process. However, the theoretical solutions to guided wave scattering problems with assumptions such as the Born approximation have led to the poor quality of the reconstructed results. Besides, the scattering signals collected from industry sectors are often noised and nonstationary. To address these issues, a novel physics-informed framework (PIF) for the quantitative reconstruction of defects by means of the integration of the data-driven method with the guided wave scattering analysis is proposed in this paper. Based on the geometrical information of defects and initial results obtained by the PIF-based analysis of defect reconstructions, a deep-learning neural network model is built to reveal the physical relationship between the defects and the noisy detection signals. This learning model is then adopted to assess and characterize the defect profiles in structures, improve the accuracy of the analytical model, and eliminate the impact of the noise pollution in the process of inspection. To demonstrate the advantages of the developed PIF for the complex defect reconstructions with the capability of denoising, several numerical examples are carried out. The results show that the PIF has greater accuracy for the reconstruction of defects

---

\* Citation: LI, Q., LIU, F. S., WANG, B., LIU, D. Z., and QIAN, Z. H. A novel physics-informed framework for reconstruction of structural defects. *Applied Mathematics and Mechanics (English Edition)*, **43**(11), 1717–1730 (2022) <https://doi.org/10.1007/s10483-022-2912-6>

† Corresponding authors, E-mails: dianzi.liu@uea.ac.uk; qianzh@nuaa.edu.cn

Project supported by the National Natural Science Foundation of China (Nos.12061131013, 12211530064, and 12172171), the Fundamental Research Funds for the Central Universities of China (Nos.NE2020002 and NS2019007), the National Natural Science Foundation of China for Creative Research Groups (No.51921003), the Postgraduate Research and Practice Innovation Program of Jiangsu Province of China (No.KYCX21\_0184), the National Natural Science Foundation of Jiangsu Province of China (No.BK20211176), the State Key Laboratory of Mechanics and Control of Mechanical Structures at Nanjing University of Aeronautics and Astronautics of China (No.MCMS-E-0520K02), and the Interdisciplinary Innovation Fund for Doctoral Students of Nanjing University of Aeronautics and Astronautics of China (No.KXKCXJJ202208)

in the structures than the analytical method, and provides a valuable insight into the development of artificial intelligence (AI)-assisted inspection systems with high accuracy and efficiency in the fields of structural integrity and condition monitoring.

**Key words** physics-informed, deep-learning, reconstruction of defects, denoising

**Chinese Library Classification** O343

**2010 Mathematics Subject Classification** 74J05, 74J20, 74J25

## 1 Introduction

In the non-destructive testing of elastic waveguide structures such as rods, plates, shells, and beams, ultrasonic guided wave detection has the advantages of convenient excitation, long propagation distance, high sensitivity to defects, and low energy consumption<sup>[1–4]</sup>. Especially, for the non-destructive testing in significant areas such as railway transportation, oil pipelines, airframe, and aircraft wings<sup>[5]</sup>, the high efficiency and high precision of ultrasonic guided wave detection are more important. Therefore, using guided waves for defect detection and reconstruction has been investigated by many researchers. As early as the beginning of this century, Rose<sup>[1]</sup> clarified that ultrasonic guided waves could be used to detect pores and weaken cohesion and delamination, and had considerable reliability. Eremin et al.<sup>[6]</sup> studied the Lamb wave properties and its changes during the cyclic loading of carbon fiber-reinforced polymer (CFRP) sandwich panels with aluminium honeycomb cores. Based on the Lamb wave analysis, the fatigue failure and tensile-compressive failure of two specimens were identified. Puthillath and Rose<sup>[7]</sup> developed a detection method of ultrasonic guided wave linear scanning, also known as G-scan, which could detect the bonding damage of the patch during the repair of the aircraft shell, such as adhesive and cohesive weaknesses similar to those found in adhesively bonded joints. Wang and Hirose<sup>[8]</sup> used the Born approximation to replace the total field near the defect with the incident field, and derived the mathematical relationship between the reflection coefficient located in the far field and the defect shape function in the form of Fourier transform pairs for the thinning defect reconstruction in the two-dimensional plate. Sikdar and Banerjee<sup>[9]</sup> used the probabilistic damage detection algorithm to identify the location and size of the disband and high-density core region in a honeycomb composite sandwich structure (HCSS) by means of ultrasonic guided waves and surface-bonded piezoelectric wafer transducers (PWTs). Da et al.<sup>[10]</sup> proposed a novel reference model-based method, called QDFT, for the quantitative reconstruction of pipeline defects with ultrasonic guided shear surface (SH)-waves in 2018. Based on the boundary integral equation, the Fourier transform pair of reflection coefficients in the wavenumber domain and the defect shape function in the spatial domain were analytically obtained by means of the Born approximation to reconstruct the defect profiles.

Although many researchers have made valuable exploration and remarkable progresses on the applications of guided waves for non-destructive testing to identify their values, it is difficult to realize high accurate and efficient defect reconstruction with the guided wave scattering theory due to the coupling of various modes in the guided wave scattering field. Moreover, the existing defect detection and reconstruction technologies need to cooperate with the signal processing system, and the actual measurement is inevitably affected by the environmental noise, which will lead to the inaccuracy of defect reconstruction. Therefore, it is time to revisit the artificial intelligent technology for the reconstruction of defects with high levels of robustness and reliability.

Artificial intelligence (AI) has been rapidly developed, and has been widely applied for solving problems<sup>[11–12]</sup>. In the field of defect detection, Munir et al.<sup>[13]</sup> applied the convolutional neural network (CNN) for noisy ultrasonic signatures to improve the classification performance of weldment defects and applicability. Wang et al.<sup>[14]</sup> proposed a rapid guided wave imaging method based on the CNN to quantitatively evaluate the corrosion damage. The artificial

neural network has also been used for the efficient extraction and selection of features in the context of a decision support system<sup>[15]</sup>. Ye and Yu<sup>[16]</sup> proposed a novel deep morphological convolutional network (DMCNet) for the feature learning of gearbox vibration signals for fault diagnosis. Virkkunen et al.<sup>[17]</sup> developed a modern deep convolutional network to detect the flaws represented by phased-array ultrasonic data. Latête et al.<sup>[18]</sup> used the faster R-CNN to identify, locate, and size the flat bottom holes (FBMs) and side-drilled holes (SDHs) in an immersed test specimen by means of a single plane wave insonification. Miorelli et al.<sup>[19]</sup> proposed a kernel-based machine learning model to achieve automatic flaw detection, localization, and characterization. Zhao et al.<sup>[20]</sup> proposed a dynamic radius support vector data description (DR-SVDD) for the fault detection of aircraft engines. In the area of computer tomography (CT), Jin et al.<sup>[21]</sup> combined the deep CNN with the filtered back projection algorithm (FBP). First, the FBP was used to process the sub-sampled sinogram for obtaining a preliminary reconstructed image. Then, the reconstructed image was used as the input data to train the CNN for the output of a high-quality reconstructed image. In order to solve the problem of multiple scattering in image reconstruction, Sun et al.<sup>[22]</sup> divided the scattering inversion process into two steps. In the first step, a theoretical model was used to design a back propagation algorithm for transforming the data in the measurement domain into the image domain. In the second step, a deep CNN with U-net structure was generated as a scattering decoder to complete the reconstruction task by using the image domain data. They showed that the deep-learning-based image reconstruction method had higher computational efficiency and reconstruction quality than other methods when dealing with multiple scattering problems. Boubilil et al.<sup>[23]</sup> combined the FBP algorithm and the PWLS iterative algorithm with the CNN to reconstruct images, and concluded that the local fusion between these two algorithms could improve the balance between the resolution and the variance in the image reconstruction process. McCann et al.<sup>[24]</sup> summarized extensive research works by deep-learning algorithms for scattering inversion, and concluded that in the field of image scattering inversion, due to the lack of sample data, the mainstream method of deep-learning algorithms for scattering inversion was to combine the traditional reconstruction algorithm with the deep-learning algorithm. Usually, traditional theoretical methods are used for pre-reconstruction, and the reconstruction results are collected as the input data to train the machine learning model for the prediction of high-quality reconstruction results.

In view of the application of deep-learning algorithms, especially the CNN algorithm in the field of image reconstruction, a quantitative defect reconstruction physics-informed framework (PIF) combining the existing theoretical model of guided wave defect reconstruction with deep-learning algorithms is proposed in this paper. With the results obtained by the PIF-based analysis of defect reconstruction as the training data, the feature representations of defect profiles are extracted by an effective deep-learning neural network. To demonstrate the ability of the developed PIF for defect reconstructions in terms of the accuracy and denoising capabilities, numerical examples are carried out to evaluate the overall performance of the intelligent model by comparison with the published results.

## 2 PIF-based analysis of defect reconstruction

The process of incident waves traveling through the thinning structures can be described in Fig. 1. First, the ultrasonic guided SH-wave is excited on the right side of the plate, and the reflection coefficient is calculated from the reflected wave signals. Following this, the inverse Fourier transform of the reflection coefficient is used to analytically obtain the shape function of the defect for defect reconstruction<sup>[8]</sup>.

The brief introduction of interactions occurred when the waves propagate in the cracked frame structure steps can be depicted as follows.

Assuming that the incident guided SH-wave in this problem has a single  $n$ th mode, propa-

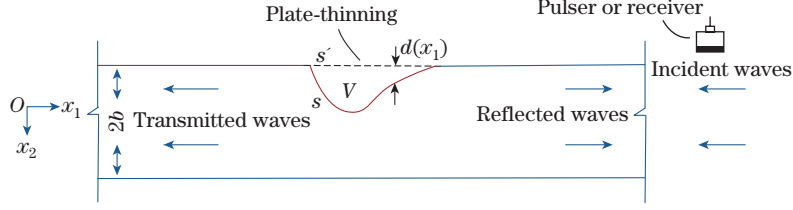


**Fig. 1** Reflection and transmission of an incident guided SH-wave by a plate thinning (color online)

gating from right to left and being reflected back by the thinning part, and the reflected wave with the same mode as the incident wave mode is observed in the far field. Starting from the wave equation in the plate and the corresponding boundary conditions<sup>[8]</sup>, the displacement field in the plate can be determined by

$$\begin{cases} \tilde{u}^{\text{inc}} = A_n^{\text{inc}} f_n(\beta_n x_2) e^{+i\xi_n x_1}, & \tilde{u}^{\text{ref}} = A_n^{\text{ref}} f_n(\beta_n x_2) e^{-i\xi_n x_1}, \\ \beta_n = n\pi/(2b), & \xi_n = \sqrt{\frac{\omega^2}{V_s^2} - \beta_n^2}, \end{cases} \quad (1)$$

where  $n$  represents the  $n$ th guided SH-wave mode, and  $n = 0, 1, 2, \dots$ .  $\tilde{u}^{\text{inc}}$  and  $\tilde{u}^{\text{ref}}$  depict the displacement fields of the incident and reflected waves, respectively.  $A_n^{\text{inc}}$  and  $A_n^{\text{ref}}$  are the amplitude coefficients of the incident and reflected waves, respectively.  $f_n(x)$  is defined by

$$f_n(x) = \begin{cases} \cos x, & n = 0, 2, 4, \\ \sin x, & n = 1, 3, 5. \end{cases} \quad (2)$$

Subsequently, the reflection coefficient is defined by

$$C^{\text{ref}} = A_n^{\text{ref}}/A_n^{\text{inc}}. \quad (3)$$

Applying the reciprocal theorem of dynamics<sup>[25]</sup> and Green's function  $\tilde{U}(\mathbf{x}, \mathbf{X})$  in the plate, the scattered displacement field is analytically derived by using the boundary integral equation as follows:

$$\tilde{u}^{\text{sca}}(\mathbf{x}) = \int_S \left( \tilde{u}^{\text{tot}}(\mathbf{X}) \mu \frac{\partial \tilde{U}(\mathbf{X}, \mathbf{x})}{\partial n(\mathbf{X})} - \mu \frac{\partial \tilde{u}^{\text{tot}}(\mathbf{X})}{\partial n(\mathbf{X})} \tilde{U}(\mathbf{X}, \mathbf{x}) \right) ds(\mathbf{X}), \quad (4)$$

where  $\tilde{u}^{\text{sca}}$  and  $\tilde{u}^{\text{tot}}$  represent the scattered and total displacement fields, respectively. As the defect boundary is free,  $\frac{\partial \tilde{u}^{\text{tot}}}{\partial n} = 0$  can be easily derived. For a weak scattering defect, the Born approximation can be used to replace the total wave displacement field  $\tilde{u}^{\text{tot}}(\mathbf{X})$  in Eq. (4) with the incident wave field  $\tilde{u}^{\text{inc}}(\mathbf{X})$ . Then, one has

$$\tilde{u}^{\text{sca}}(\mathbf{x}) \approx \int_S \tilde{u}^{\text{inc}}(\mathbf{X}) \mu \frac{\partial \tilde{U}(\mathbf{X}, \mathbf{x})}{\partial n(\mathbf{X})} ds(\mathbf{X}). \quad (5)$$

Using the Gauss theorem, the surface integral of the defect is converted into the integral over the volume of the defect as follows:

$$\tilde{u}^{\text{sca}}(\mathbf{x}) \approx \int_V \left( -k^2 \tilde{u}^{\text{inc}}(\mathbf{X}) \mu \tilde{U}(\mathbf{X}, \mathbf{x}) + \mu \frac{\partial \tilde{U}(\mathbf{X}, \mathbf{x})}{\partial X_i} \frac{\partial \tilde{u}^{\text{inc}}(\mathbf{X})}{\partial X_i} \right) dV(\mathbf{X}), \quad (6)$$

where Green's function  $\tilde{U}(\mathbf{x}, \mathbf{X})$  represents the anti-plane displacement at the field point  $\mathbf{x} = (x_1, x_2)$  due to a harmonic point force exerted at the source point  $\mathbf{X} = (X_1, X_2)$  in an intact plate. Green's function  $\tilde{U}(\mathbf{x}, \mathbf{X})$  satisfies the following equation of motion:

$$\nabla^2 \tilde{U}(\mathbf{x}, \mathbf{X}) + k^2 \tilde{U}(\mathbf{x}, \mathbf{X}) = -\delta(x - X)/\mu. \quad (7)$$

The traction free boundary condition can be written as

$$\tilde{T}(\mathbf{x}, \mathbf{X}) = \mu \frac{\partial}{\partial n(\mathbf{x})} \tilde{U}(\mathbf{x}, \mathbf{X}) = 0 \quad \text{on} \quad x_2 = \pm b, \quad (8)$$

where  $k = \omega/V_S$  is the shear wave number, and  $\frac{\partial(\cdot)}{\partial n}$  indicates the normal derivative. The solution to Eq. (7), that is Green's function  $\tilde{U}(\mathbf{x}, \mathbf{X})$ , can be expressed as

$$\begin{aligned} \tilde{U}(\mathbf{x}, \mathbf{X}) &= \tilde{U}^{\text{inc}}(\mathbf{x}, \mathbf{X}) + \tilde{U}^{\text{ref}}(\mathbf{x}, \mathbf{X}) \\ &= \frac{1}{4\pi\mu} \int_{-\infty}^{\infty} \frac{e^{-R|x_2-X_2|}}{R} e^{-i\xi(x_1-X_1)} d\xi + \frac{1}{4\pi\mu} \int_{-\infty}^{\infty} (A^+ e^{-Rx_2} + A^- e^{+Rx_2}) e^{-i\xi(x_1-X_1)} d\xi, \end{aligned} \quad (9)$$

where  $\tilde{U}^{\text{inc}}(\mathbf{x}, \mathbf{X})$  is the fundamental solution,  $\tilde{U}^{\text{ref}}(\mathbf{x}, \mathbf{X})$  means the additional term, and  $R = \sqrt{\xi^2 - k^2}$  ( $|\xi| \geq k$ ) or  $i\sqrt{k^2 - \xi^2}$  ( $|\xi| \leq k$ ).

Substituting Eq. (9) into Eq. (8), the undetermined amplitudes  $A^+$  and  $A^-$  can be solved. Thus,  $\tilde{U}(\mathbf{x}, \mathbf{X})$  can be rewritten as

$$\begin{aligned} \tilde{U}(\mathbf{x}, \mathbf{X}) &= \frac{1}{4\pi\mu} \int_{-\infty}^{\infty} \left( \frac{e^{-R|x_2-X_2|}}{R} + \frac{e^{-2Rb}}{2R(1+e^{-2Rb})} (e^{-RX_2} - e^{+RX_2})(e^{-Rx_2} - e^{+Rx_2}) \right. \\ &\quad \left. + \frac{e^{-2Rb}}{2R(1-e^{-2Rb})} (e^{-RX_2} + e^{+RX_2})(e^{-Rx_2} + e^{+Rx_2}) \right) e^{-i\xi(x_1-X_1)} d\xi. \end{aligned} \quad (10)$$

For  $|x_1| \geq |X_1|$ , the far-field expression for Green's function is given as

$$\tilde{U}(\mathbf{x}, \mathbf{X}) \cong \tilde{U}^{\text{far}}(\mathbf{x}, \mathbf{X}) = \frac{i}{4b\mu\xi_0} e^{-i\xi_0|x_1-X_1|} - \sum_j \frac{i}{2b\mu\xi_j} f_j(\beta_j x_2) f_j(\beta_j X_2) e^{-i\xi_j|x_1-X_1|}, \quad (11)$$

where the functions  $f_n(x)$  is defined in Eq. (2).

Based on the far field approximation<sup>[8]</sup>, Green's function  $\tilde{U}(\mathbf{x}, \mathbf{X})$  in a traction-free plate waveguide for SH-waves can be expressed as

$$\tilde{U}(\mathbf{x}, \mathbf{X}) \approx \tilde{U}^{\text{far}}(\mathbf{x}, \mathbf{X}) = -\frac{i}{2b\mu\xi_n} \cos(\beta_n x_2) \cos(\beta_n X_2) e^{-i\xi_n(x_1-X_1)}. \quad (12)$$

Substituting Eqs. (1) and (12) into Eq. (6) yields the displacement field of the reflected wave as follows:

$$\tilde{u}^{\text{ref}}(\mathbf{x}) = \frac{i}{2b} A_n^{\text{inc}} \int_V \frac{\xi_n^2 + k^2 \cos(2\beta_n X_2)}{\xi_n} e^{2i\xi_n X_1} dV(\mathbf{X}) \times \cos(\beta_n x_2) e^{-i\xi_n x_1}. \quad (13)$$

Comparing Eq. (1) with Eq. (13), it is noted that the integral term in Eq. (13) corresponds to the reflection coefficients, and the volume integral represents the multiple integrals. Thus, one obtains

$$C^{\text{ref}} = \frac{A_n^{\text{ref}}}{A_n^{\text{inc}}} = \frac{i}{2b} \frac{\xi_n^2 + k^2}{\xi_n} \int_{-\infty}^{\infty} d(X_1) e^{2i\xi_n X_1} dX_1, \quad (14)$$

where  $C^{\text{ref}}$  is the reflection coefficients, and  $d(X_1)$  describes the defect profile.

In Eq. (14), it can be observed that  $C^{\text{ref}}$  and  $d(X_1)$  form a Fourier transform pair. Applying the inverse Fourier transform on Eq. (14), the defect profile  $d(X_1)$  is determined by

$$d(X_1) = \frac{1}{2\pi} \int_{-\infty}^{+\infty} \frac{-2ib\xi_n}{\xi_n^2 + k^2} C^{\text{ref}} e^{-2i\xi_n X_1} d(2\xi_n). \quad (15)$$

As  $d(X_1)$  is described in the spatial domain and  $C^{\text{ref}}$  is in the wavenumber domain, the defect reconstruction method aforementioned is called the wavenumber spatial transformation (WNST) method<sup>[8]</sup>. To derive Eq. (15), there are some assumptions applied including the thinning defect as a weak scattering source ( $d \ll b$ ), the Born approximation to replace the total field near the defect with the incident field, and the far field approximation used for calculating Green's function of the bounded plate. These approximations can help simplify the physics-informed formulations for defect reconstruction in an efficient way, while it is inevitable to introduce model errors and reduce the accuracy of reconstruction results.

### 3 A novel physics-informed framework

In order to improve the accuracy of the physics-informed modeling and eliminate the impact of noise pollution in the process of defect inspection and reconstruction, the fusion of a data-driven CNN with the physics-informed analysis by means of the WNST method, called the WNSTConvNet framework, is proposed in this paper for defect reconstruction.

The physical process of using ultrasonic waves to detect defects can be described as follows. In the process of propagation of sound waves along the medium, scattering will occur when encountering defects, resulting in the transmission wave field and reflection wave field. Using the defect information from the transmitted and reflected signals, defect detection or reconstruction can be achieved. Therefore, guided wave defect reconstruction can be attributed to a scattering problem. For a scattering problem, it can be simply expressed by

$$y = Tx + \xi, \quad (16)$$

where  $x$  represents the scattering source that is assumed as a thinning defect in this study,  $y$  represents the scattering field signal,  $T$  is an operator with properties dependent on the specific scattering problem, and  $\xi$  is the error. The task of inverse scattering problems is to calculate  $x$  based on  $y$ . The traditional methods to solve this class of problems are divided into two categories. One aims to directly construct the inverse problem model, such as the WNST method aforementioned. The corresponding mathematical formulation can be given as

$$x = \hat{T}^{-1}y, \quad (17)$$

where  $\hat{T}^{-1}$  is the theoretical reconstruction operator. The advantage of this method lies in that for the reconstruction of defects in simple structures, the calculation of the inverse scattering can be performed in a short time. The disadvantage of this method is the difficulty in obtaining accurate results due to the ill-posed inverse problems. In particular, when the scattering problem becomes complex, it will be extremely difficult to develop the reconstructed model, and thus the reconstruction accuracy and reliability will be affected. The other is iterative-based methods for solving inverse scattering problems, e.g., the QDFT<sup>[10]</sup> with the mathematical formulation as follows:

$$O\{y\} = \arg \min_x f(T(x), y), \quad (18)$$

where the function  $f$  is used to characterize the error between  $T(x)$  and  $y$ . The iterative-based method has the ability to obtain accurate results. However, its efficiency of defect reconstruction is low, owing to a lot of computational time required by the iterative process.

In this paper, the approach based on machine learning is proposed to solve the inverse scattering problem. The inverse problem model, which is constructed through the training session, can be created in a mathematical form as follows:

$$L = \arg \min_{\theta} \sum_{n=1}^N M(x_n, H_{\theta}(y_n)) + r(\theta), \quad (19)$$

where  $x_n$  is the exact defect;  $y_n$  denotes the reflection coefficients; the symbol  $M$  is the loss function for characterizing the difference between samples  $x_n$  and  $H_{\theta}(y_n)$ ;  $H_{\theta}$  is the neural network built for solving the inverse problem;  $\theta$  is the parameter in the neural network, and is iteratively updated during the entire training process;  $N$  represents the total number of pairs in training samples;  $r$  is a regularization term, which prevents over-fitting and also limits the value of the parameter  $\theta$  to reduce the complexity of the trained network model  $H_{\theta}$ . After the training is completed, the network can achieve a high reconstruction accuracy with a high level of efficiency.

In order to make full use of the existing defect reconstruction theory, the integration of the theoretical model (WNST) with machine learning methods is proposed in a manner of local fusion to efficiently and accurately solve the defect reconstruction problem by using the ultrasonic guided waves. The mechanism of this novel WNSTConvNet framework can be mathematically described as

$$L = \arg \min_{\theta} \sum_{n=1}^N P(x_n, L_{\theta}(\hat{T}^{-1}y_n)) + g(\theta), \quad (20)$$

where the training sample pair is  $(x_n, \hat{T}^{-1}y_n)$ , in which  $x_n$  is the exact defect and  $\hat{T}^{-1}y_n$  represents the defect constructed by the physics-informed construction model. The mean square error (MSE) is selected to evaluate the performance function  $P$  during the training session.  $L_{\theta}$  is the WNSTConvNet framework, but its argument is the pre-reconstruction. The regularization function  $L_2$  is adopted to determine the regularization term  $g(\theta)$  to reduce the complexity of the model and prevent overfitting. In this study, the initial results obtained by the physics-informed model are treated as the training data for the generation of the machine learning model to improve the accuracy of defect reconstruction. The developed framework architecture and training process designed in this paper are shown in Fig. 2.

Since the input samplings are one-dimensional signals, a one-dimensional deep-learning network is constructed. The training process is depicted in Fig. 2. Once the training session is completed, the deep-learning network has the ability to efficiently predict the high-quality reconstructed defect for a given defect signal  $\hat{T}^{-1}y_n$ . In this developed network, the ReLU<sup>[26]</sup> activation function is used for each convolutional layer. In order to address the problem of gradient disappearance encountered during the training session, the batch normalization is performed before the activation to improve the training efficiency. To prevent overfitting, a dropout layer<sup>[27]</sup> is added at the end of the network to discard some training parameters and improve its robustness. Based on the fusion of physics-informed calculations and predictions by the deep-learning intelligent network, the developed WNSTConvNet framework, which has been implemented in Python by using the TensorFlow library, demonstrates the outperformance over its rivals for defect reconstructions throughout the complex examples in the following section.

#### 4 Experimental validation

In this paper, two sets of sample data are generated to train the intelligent network in the WNSTConvNet framework for defect reconstruction with high levels of accuracy and robustness.

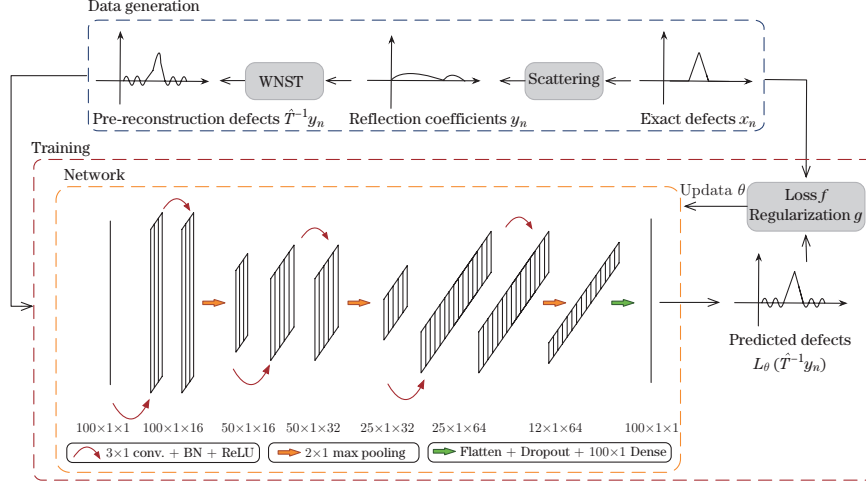


**Fig. 2** Schematic illustration of the reconstruction pipeline and the WNSTConvNet convolutional architecture (color online)

#### 4.1 Data preparation

A mixed defect dataset, containing 1 200 defect profiles including randomly isosceles triangular defects, rectangular defects, and stepped defects, is created. For the input data of the WNSTConvNet framework, it is obtained by the analytical calculations as follows. First, the reflection coefficients of the 0th SH-wave mode corresponding to the exact defect are obtained by the modified boundary element method (MBEM)<sup>[28]</sup> for all the examples in this paper. In practice, multi-dimensional Fourier transforms and frequency-wavenumber filtering can be applied to the incident wave removal and mode separation<sup>[29-30]</sup>. Following that, the shape function  $d(X_1)$  of the defect is constructed by the WNST (see Eqs. (14) and (15)), which deals with the input data required. Among 1 200 sets of sampling data, the dataset split ratio of 0.9 is applied.

To further improve the performance of network and reconstruct more complex defects, the augmented dataset is generated. First, the pre-reconstruction isosceles triangular and rectangular defects with random sizes and shapes are created by using the WNST method formulated by Eqs. (14) and (15). Then, the augmented data are generated by randomly shifting the signals in the horizontal direction. Summarily, there are 2 800 sets of sampling data including 800 original inputs and 2 000 augmented data for the network training, verification, and testing.

#### 4.2 Experimental results

Once the network training is completed, the reconstruction of defects with simple defective geometries, stepped geometries, and a mixed type of profiles will be conducted. In order to quantify the difference between the reconstructed defect and the real defect, the signal-to-noise ratio (SNR)<sup>[31]</sup> used as the loss function to measure the reconstruction quality is proposed as follows:

$$f_{\text{SNR}}(\mathbf{x}, \hat{\mathbf{x}}) \triangleq \max_{a \in \mathbb{R}} \left( 10 \lg \left( \frac{\|\mathbf{x}\|_{l_2}^2}{\|\mathbf{x} - a\hat{\mathbf{x}}\|_{l_2}^2} \right) \right), \quad (21)$$

where  $\mathbf{x}$  is the real defect, and  $\hat{\mathbf{x}}$  is the predicted reconstruction of defect. A higher SNR value corresponds to a better reconstruction. Note that the vector  $\mathbf{x}$  or  $\hat{\mathbf{x}}$  used to characterize the defect shape in this study is actually the spatial distribution of the defect shape in the entire detection range, including the defect region and the defect-free region.

#### 4.2.1 Mixed defect datasets

The CNN is initially constructed during the training session using the mixed type of defects described in Subsection 4.1. The reconstructed results of triangular defects, rectangular defects, and stepped defects are shown in Fig. 3, and the values of  $f_{\text{SNR}}$  obtained are provided in Table 1. It is noted that the WNSTConvNet framework has the ability to achieve defect reconstruction with a high level of accuracy. Especially, for rectangular and stepped defects, the SNR value reaches about 28 dB. The average SNR value of the reconstruction results across the entire testing dataset is 23.95 dB, which enables the improvement of reconstruction results and leads to nearly 200% higher precision than the results obtained by the WNST method.

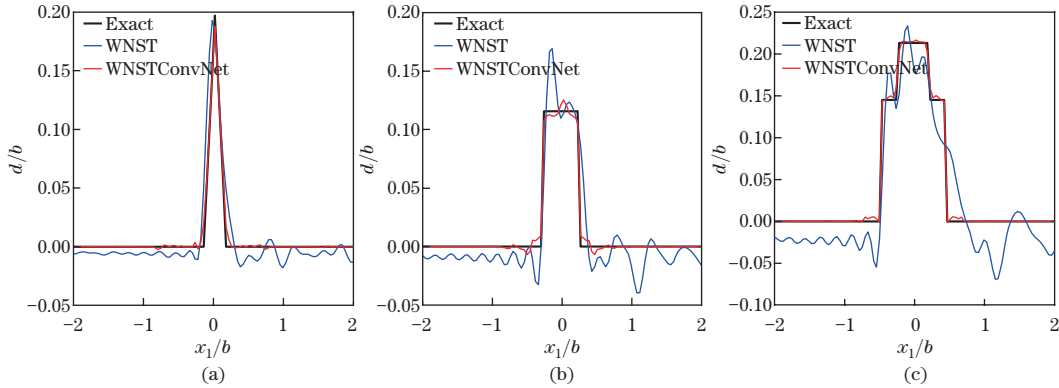


**Fig. 3** Reconstruct triangular defect (a), rectangular defect (b), and stepped defect (c) under the proposed WNSTConvNet framework (color online)

**Table 1** Comparison of SNR (dB) values of the reconstruction results obtained by the WNST method and the WNSTConvNet framework

Reconstruction method	Triangular defect	Rectangular defect	Stepped defect	Average SNR over the dataset
WNST	9.25	8.13	7.88	8.20
WNSTConvNet	20.29	28.40	28.03	23.95

#### 4.2.2 Augmented datasets

Insufficient data is a critical issue that limits the application of machine learning methods in engineering subjects. In this situation, the generation of an augmented dataset by the data augmentation method can fully dig out the information hidden owing to the limited data. In this experiment, the 2800 sets of augmented data are used to train and verify the intelligent network. During the training session, the hyper parameters of the network are finely tuned to reconstruct the asymmetric defects created by the combination of triangular and rectangular defects to improve the network with better generalization performance. The reconstruction results of two asymmetric combined defects are shown in Fig. 4(a) and Fig. 4(b), respectively. In Table 2, the obtained SNR values are provided, along with the results from the WNST method for comparison. It can be observed that the network trained by using triangular defects, rectangular defects, and their augmented data has the ability to reconstruct general asymmetric defects, and the reconstruction accuracy has been remarkably improved in comparison with the results from the WNST method. Therefore, it can be concluded that the network designed by the WNSTConvNet framework has demonstrated good generalization ability throughout the examples and the developed data-driven model, that fuses the geometrical information of defects and initial results by the physics-informed analysis of defect reconstructions, has the capability to efficiently and effectively assess and characterize defects with complex profiles.

The major bottleneck in engineering applications of deep-learning is the limited amounts of effective data. In this study, the data-driven network model is trained by using defects with the basis profiles to realize the reconstruction of defects with complex profiles. However, it is very challenging to achieve the reconstruction with a high level of precision. To address this issue, additional 28 (about 1% of the original number) defects with complex profiles representing the combination of triangular and rectangular shapes are added to the training set for the improvement of the network. This also empowers the network with the learning capability by taking the advantage of transfer learning<sup>[32]</sup>. Therefore, there are 2828 sets of training data to build the effective machine learning model for the high-precision defect reconstruction. The reconstruction results of complex defect profiles are shown in Fig. 4(c), and the SNR value of the reconstruction result, which is 22.52 dB, is given in Table 3.

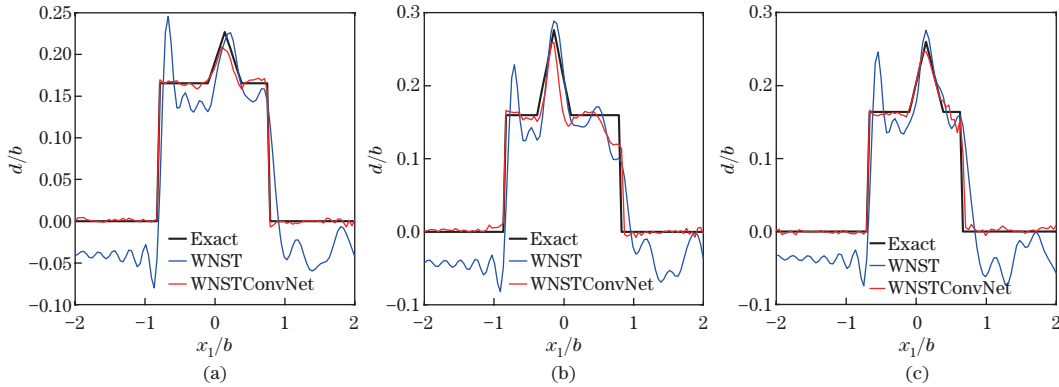


**Fig. 4** Two reconstruction samples using the neural network trained with 2800 augmentation samples: (a) Sample I and (b) Sample II. (c) One reconstruction sample using the neural network trained with 2828 augmentation samples including 28 combination defects samples (Sample III) (color online)

**Table 2** Comparison of the SNR (dB) values of the reconstruction results obtained by the WNST method and WNSTConvNet framework

Reconstruction method	Sample I	Sample II	Average SNR over the dataset
WNST	8.79	8.87	7.54
WNSTConvNet	21.62	16.65	17.03

**Table 3** SNR (dB) values of reconstruction results of the neural network trained with additional 28 combination defects samples

Reconstruction method	Sample III	Average SNR over the dataset
WNST	7.64	7.54
WNSTConvNet	22.52	21.33

#### 4.2.3 Reconstruction of noisy defects

In order to ensure the robustness of this data-driven defect reconstruction model, the network trained by the augmented datasets, which include 2800 defect samples, is constructed to detect defects by using signals in Gaussian white noise. First, the Gaussian white noise with an SNR of 15 dB is added to the input signals of the WNSTConvNet framework. Then, the trained deep-learning network is examined for the denoising capability and defect reconstruction ability. In Fig. 5(a), the defects with the noisy fringe and the predicted results by the WNST

method and the developed deep-learning network are provided. Table 4 shows the average SNR values of the reconstructed results over the entire testing data by the WNST method and the WNSTConvNet framework. It is noted that the accuracy is improved by nearly 100%, which demonstrates that the WNSTConvNet framework has a greater self-learning denoising capability. In order to further improve the denoising capability of the WNSTConvNet framework, a dataset of 2800 augmented signals containing 15 dB of Gaussian white noise is labeled as the training data to generate a more powerful and intelligent network. It can be observed that the denoising capability of the updated WNSTConvNet framework is significantly improved. The reconstructed defect by the WNSTConvNet framework is in good agreement with the real defect and outperforms the result by the WNST method (see Fig. 5(b)), and the accuracy of defect reconstruction can reach 17.66 dB (see Table 5).

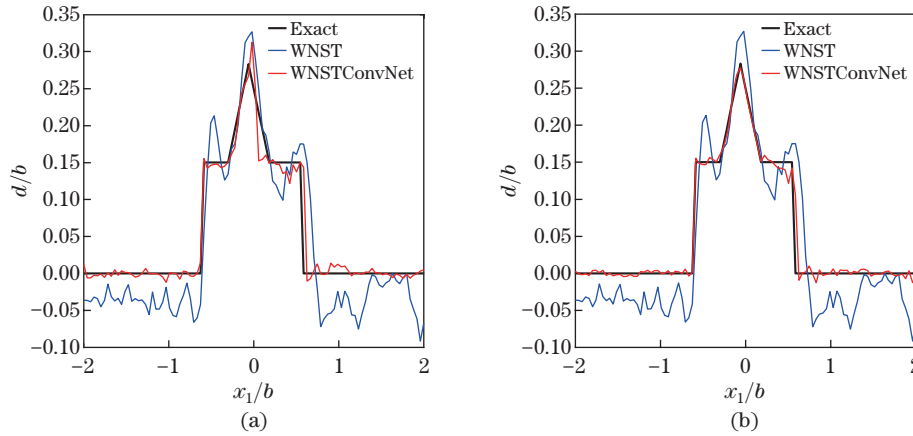


**Fig. 5** (a) Reconstruction results of defects from noisy signals by using the neural network trained with 2800 augmentation samples. (b) Reconstruction results of defects from noisy signals by using the neural network trained with 2800 augmentation noise-containing samples (color online)

**Table 4** SNR (dB) values of the reconstruction results of defects from noisy signals by using the neural network trained with 2800 augmentation samples

Reconstruction method	Sample I	Average SNR over the dataset
WNST	7.35	7.13
WNSTConvNet	14.62	13.86

**Table 5** SNR (dB) values of the reconstruction results of defects from noisy signals by using the neural network trained with 2800 augmentation noise-containing samples

Reconstruction method	Sample II	Average SNR over the dataset
WNST	7.35	7.13
WNSTConvNet	18.04	17.66

## 5 Discussion

The simulation results prove the effectiveness and robustness of the WNSTConvNet framework for defect reconstruction with a remarkable denoising capability. This is of great significance to the area of high-precision defect detection in engineering. At the same time, the great

robustness of the WNSTConvNet framework can be demonstrated by the effective removal of samples mixed with noise during the defect reconstruction process. Therefore, it can improve the quality of reconstructed defects. Besides, removing the noise from the signals representing the features of the defect-free area also benefits the identification of the exact location of defects. It is noted that it takes less than one second to achieve the defect reconstruction with a high level of accuracy by using the WNSTConvNet framework for the reconstruction of defects.

The limitation of the defect reconstruction method based on the supervised learning algorithm lies in the fact that the generated network architecture can only work on the information that is either provided in the initial guess or extracted from the training data. According to the first experimental test, one of the solutions to address this problem in practical applications is to train the neural network with datasets of a variety of typical geometrical information. Moreover, a classification layer followed by the reconstruction layer can be elaborately added in the design of network architecture so that the ensemble of different types of pre-reconstruction defects predicted by the corresponding CNN can be further developed in the network architecture for the improvement of computational accuracy. Another constraint on using neural networks to reconstruct defects is the need for a large amount of training data to guarantee the reliability of the predicted results. At present, using simulation results as a source of data to train a neural network is a feasible method in practice to solve the data problems.

The WNSTConvNet framework proposed in this paper is the fusion of the physics-informed wave scattering analysis and the data-driven approach for defect reconstruction, and its working mechanism has not been constrained by the theoretical model and the machine learning model. In this paper, the WNST and the CNN are selected as representative models to demonstrate the effectiveness and correctness of the proposed framework for the reconstruction of complex defects.

## 6 Conclusions

This paper proposes a novel physics-informed quantitative defect reconstruction (WNSTConvNet) framework, which integrates the WNST method with a CNN in a local fusion manner. Throughout three complex experiments by comparison of the reconstruction results between the WNSTConvNet ensemble and the WNST method, it is demonstrated that the WNSTConvNet framework is more effective, accurate, and robust for the reconstruction of complex defects. The results obtained by the WNSTConvNet framework have an average reconstruction accuracy of 20 dB for randomly isosceles triangular defects, rectangular defects, and stepped defects, demonstrating its good generalization performance. Especially, for the reconstruction of rectangular defects and stepped defects, the accuracy of reconstructions by the WNSTConvNet framework is improved by nearly 200% than that by the WNST method. Moreover, considering the signal with the Gaussian noise for the combined defect profiles, the WNSTConvNet framework has a great denoising capability, which proves that the developed framework has good robustness for the reconstruction of defects. Usually, the defect reconstruction process by the WNSTConvNet framework can be completed within 1 s. Therefore, it is a high-precision and high-efficiency quantitative defect reconstruction technique in comparison with the analytical methods. In future work, experimental tests will be performed as an alternative to the numerical simulations for the validation of the defect reconstruction method. Currently, the proposed framework has provided both useful guidelines to experimental tests throughout the numerical examples and valuable insights into the development of AI-assisted inspection systems with high accuracy and efficiency in the fields of structural health monitoring and product life cycle prediction.

**Open Access** This article is licensed under a Creative Commons Attribution 4.0 International License, which permits use, sharing, adaptation, distribution and reproduction in any medium or format, as long as you give appropriate credit to the original author(s) and the source, provide a link

to the Creative Commons licence, and indicate if changes were made. To view a copy of this licence, visit <http://creativecommons.org/licenses/by/4.0/>.

## References

- [1] ROSE, J. L. A baseline and vision of ultrasonic guided wave inspection potential. *Journal of Pressure Vessel Technology*, **124**, 273–282 (2002)
- [2] BAI, H., SHAH, A. H., POPPLEWELL, N., and DATTA, S. K. Scattering of guided waves by circumferential cracks in composite cylinders. *International Journal of Solids & Structures*, **39**, 4583–4603 (2002)
- [3] SU, Z., YE, L., and LU, Y. Guided lamb waves for identification of damage in composite structures: a review. *Journal of Sound and Vibration*, **295**, 753–780 (2006)
- [4] DA, Y. H., WANG, B., LIU, D. Z., and QIAN, Z. H. An analytical approach to reconstruction of axisymmetric defects in pipelines using  $T(0, 1)$  guided waves. *Applied Mathematics and Mechanics (English Edition)*, **41**(10), 1479–1492 (2020) <https://doi.org/10.1007/s10483-020-2661-9>
- [5] QIU, L., YUAN, S., MEI, H., and FANG, F. An improved Gaussian mixture model for damage propagation monitoring of an aircraft wing spar under changing structural boundary conditions. *Sensors*, **16**, 291 (2016)
- [6] EREMIN, A. V., BURKOV, M. V., BYAKOV, A. V., LYUBUTIN, P. S., PANIN, S. V., and KHIZHNYAK, S. A. Investigation of acoustic parameters for structural health monitoring of sandwich panel under cyclic load. *Key Engineering Materials*, **712**, 319–323 (2016)
- [7] PUTHILLATH, P. and ROSE, J. L. Ultrasonic guided wave inspection of a titanium repair patch bonded to an aluminum aircraft skin. *International Journal of Adhesion and Adhesives*, **30**, 566–573 (2010)
- [8] WANG, B. and HIROSE, S. Inverse problem for shape reconstruction of plate-thinning by guided SH-waves. *Materials Transaction*, **53**, 1782–1789 (2012)
- [9] SIKDAR, S. and BANERJEE, S. Identification of disbond and high density core region in a honeycomb composite sandwich structure using ultrasonic guided waves. *Composite Structures*, **152**, 568–578 (2016)
- [10] DA, Y., DONG, G., WANG, B., LIU, D., and QIAN, Z. A novel approach to surface defect detection. *International Journal of Engineering Science*, **133**, 181–195 (2018)
- [11] ARRIDGE, S., MAASS, P., ÖKTEM, O., and SCHONLIEB, C. B. Solving inverse problems using data-driven models. *Acta Numerica*, **28**, 1–174 (2019)
- [12] AVCI, O., ABDELJABER, O., KIRANYAS, S., HUSSEIN, M., GABBOUJ, M., and INMAN, D. J. A review of vibration-based damage detection in civil structures: from traditional methods to machine learning and deep learning applications. *Mechanical Systems and Signal Processing*, **147**, 107077 (2021)
- [13] MUNIR, N., KIM, H. J., PARK, J., SONG, S. J., and KANG, S. S. Convolutional neural network for ultrasonic weldment flaw classification in noisy conditions. *Ultrasonics*, **94**, 74–81 (2019)
- [14] WANG, X. C., LIN, M., LI, J., TONG, J. K., HUANG, X. J., LIANG, L., FAN, Z., and LIU, Y. Ultrasonic guided wave imaging with deep learning: applications in corrosion mapping. *Mechanical Systems and Signal Processing*, **169**, 108761 (2022)
- [15] CRUZ, F. C., SIMASFILHO, E. F., ALBUQUERQUE, M. C. S., SILVA, I. C., FARIAS, C. T. T., and GOUVEA, L. L. Efficient feature selection for neural network based detection of flaws in steel welded joints using ultrasound testing. *Ultrasonics*, **73**, 1–8 (2017)
- [16] YE, Z. and YU, J. Deep morphological convolutional network for feature learning of vibration signals and its applications to gearbox fault diagnosis. *Mechanical Systems and Signal Processing*, **161**, 107984 (2021)
- [17] VIRKKUNEN, I., KOSKINEN, T., JESSEN-JUHLER, O., and RINTA-AHO, J. Augmented ultrasonic data for machine learning. *Journal of Nondestructive Evaluation*, **40**, 1–11 (2021)
- [18] LATÊTE, T., GAUTHIER, B., and BELANGER, P. Towards using convolutional neural network to locate, identify and size defects in phased array ultrasonic testing. *Ultrasonics*, **115**, 106436 (2021)

- 
- [19] MIORELLI, R., KULAKOVSKYI, A., CHAPUIS, B., D'ALMEIDA, O., and MESNIL, O. Supervised learning strategy for classification and regression tasks applied to aeronautical structural health monitoring problems. *Ultrasonics*, **113**, 106372 (2021)
  - [20] ZHAO, Y. P., XIE, Y. L., and YE, Z. F. A new dynamic radius SVDD for fault detection of aircraft engine. *Engineering Applications of Artificial Intelligence*, **100**, 104177 (2021)
  - [21] JIN, K. H., MCCANN, M. T., FROUSTEY, E., and UNSER, M. Deep convolutional neural network for inverse problems in imaging. *IEEE Transactions on Image Processing*, **26**, 4509–4522 (2017)
  - [22] SUN, Y., XIA, Z., and KAMILOV, U. S. Efficient and accurate inversion of multiple scattering with deep learning. *Optics Express*, **26**, 14678–14688 (2018)
  - [23] BOUBLIL, D., ELAD, M., SHTOK, J., and ZIBULEVSKY, M. Spatially-adaptive reconstruction in computed tomography using neural networks. *IEEE Transactions on Medical Imaging*, **34**, 1474–1485 (2015)
  - [24] MCCANN, M. T., JIN, K. H., and UNSER, M. Convolutional neural networks for inverse problems in imaging: a review. *IEEE Signal Processing Magazine*, **34**, 85–95 (2017)
  - [25] ACHENBACH, J. A. and ACHENBACH, J. D. *Reciprocity in Elastodynamics*, Cambridge University Press, Cambridge (2003)
  - [26] NAIR, V. and HINTON, G. E. Rectified linear units improve restricted Boltzmann machines. *Proceedings of the 27th International Conference on Machine Learning (ICML-10)*, International Machine Learning Society, Haifa, 807–814 (2010)
  - [27] YOO, H. J. Deep convolution neural networks in computer vision: a review. *IEIE Transactions on Smart Processing and Computing*, **4**, 35–43 (2015)
  - [28] YANG, C., WANG, B., and QIAN, Z. Three-dimensional modified BEM analysis of forward scattering problems in elastic solids. *Engineering Analysis with Boundary Elements*, **122**, 145–154 (2021)
  - [29] FLYNN, E. B., CHONG, S. Y., JARMER, G. J., and LEE, J. R. Structural imaging through local wavenumber estimation of guided waves. *NDT & E International*, **59**, 1–10 (2013)
  - [30] CAI, J., SHI, L., and QING, X. P. A time-distance domain transform method for Lamb wave dispersion compensation considering signal waveform correction. *Smart Materials and Structures*, **22**, 105024 (2013)
  - [31] BOUBLIL, D., ELAD, M., SHTOK, J., and ZIBULEVSKY, M. Spatially-adaptive reconstruction in computed tomography using neural networks. *IEEE Transactions on Medical Imaging*, **34**, 1474–1485 (2015)
  - [32] OQUAB, M., BOTTOU, L., LAPTEV, I., and SIVIC, J. Learning and transferring mid-level image representations using convolutional neural networks. *Proceedings of the IEEE Conference on Computer Vision and Pattern Recognition*, IEEE, Columbus (2014)